I&EC research
Industrial & Engineering Chemistry Research

Article

Cite This: Ind. Eng. Chem. Res. 2019, 58, 5838−5850

pubs.acs.org/IECR

Operational Optimization of Processes with Multistream Heat Exchangers Using Data-Driven Predictive Modeling

Harsha N. Rao, Sajitha K. Nair, and Iftekhar A. Karimi*

Department of Chemical & Biomolecular Engineering, National University of Singapore, 4 Engineering Drive 4, Singapore 117585

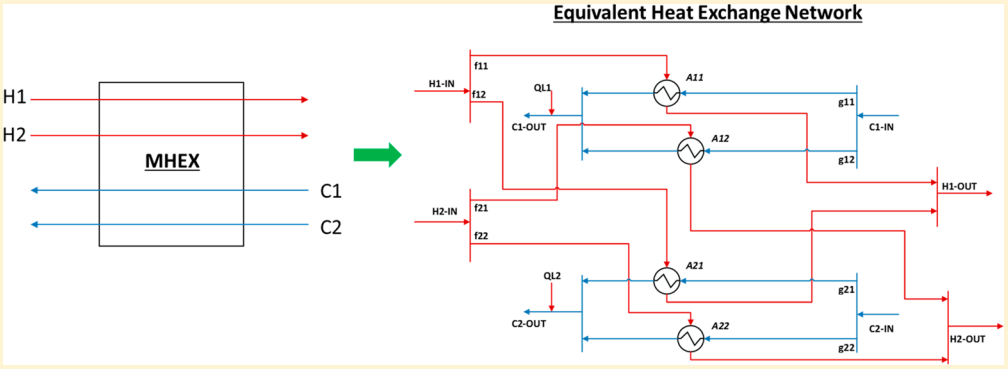

ABSTRACT: Multistream heat exchangers (MHEXs) facilitate simultaneous heat exchange between multiple streams and are mainly used in energy-intensive cryogenic processes. Reducing the energy consumption of existing processes with MHEXs is important, but system-wide operational optimization necessitates that the heat-transfer parameters of the MHEXs are known. However, most MHEXs are practically black-boxes due to their proprietary designs and complex geometry. In this work, we present a procedure for the operational optimization of processes with MHEXs. Our procedure involves the development of a predictive model for MHEXs as the first step, followed by the illustration of operational optimization. We begin with the development of a data-driven nonlinear programming (NLP) model to synthesize an equivalent network of simple two-stream heat exchangers that best represents the operation of an MHEX. We then demonstrate our predictive modeling procedure on the main cryogenic heat exchanger (MCHE) from an existing natural gas liquefaction plant. Finally, we use the equivalent network of two-stream exchangers in the operational optimization of an example C3MR process.

INTRODUCTION

A multistream heat exchanger (MHEX) is a compact equipment used to achieve simultaneous heat exchange among multiple streams. MHEXs are generally employed in capital- and energy-intensive processes such as air separation and natural gas (NG) processing/liquefaction and often involve phase changes of multicomponent mixtures.[1,2]

MHEXs usually have proprietary designs with complex flow channels. Their favorable features include heat transfer with small temperature approaches (1−3 K),[3] high heat-transfer coefficients, flexibility in flow arrangements, and reliability over a broad range of pressures. While the plate and fin and spiral wound are the most commonly preferred types of MHEXs, multipass shell and tube heat exchangers are also employed. Normally, MHEXs have a series of sections, called bundles (Figure 1). For example, a spiral-wound MHEX has multiple bundles, each with several concentric rows of tubes spirally coiled around the central axis of the shell. Typically, the high-pressure hot streams pass through separate concentric sets of tubes and traverse multiple bundles, and the low-pressure refrigerant flows down the shell side traversing all the bundles in a sequence.[2] In fact, each bundle can be treated as an independent MHEX with its own set of exchanging streams (Figure 1).

Consider an existing process (Figure 2) with multiple MHEXs. In order to optimize its entire operation, we must be able to model and simulate all of its existing units. Hence, it is logical that we need to develop a reliable predictive/operational model for each MHEX, a model which predicts the response of the MHEX to variations in feed flows and conditions and ambient temperature. However, developing a generic predictive model for the operation of an MHEX is difficult due to the unknown proprietary designs and complex flow patterns.[2] Without such a model, the plant personnel must rely on heuristics and experience to vary individual process variables.

The literature on MHEXs has mainly focused on the development of models for process simulation and design. Kamath et al.[5] developed an equation-oriented model for MHEXs, which uses the pinch concept to ensure minimum

Special Issue: Frameworks for Process Intensification and Modularization

Received: October 24, 2018
Revised: January 5, 2019
Accepted: January 16, 2019
Published: January 16, 2019

DOI: 10.1021/acs.iecr.8b05270
Ind. Eng. Chem. Res. 2019, 58, 5838−5850

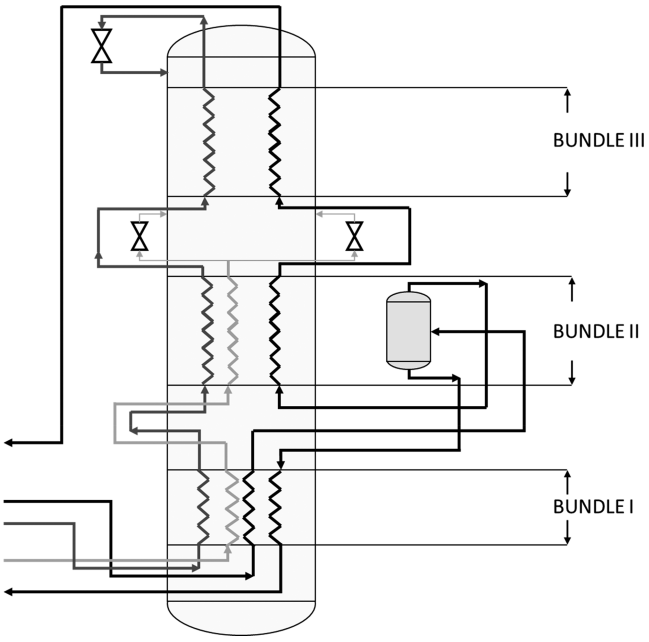

Figure 1. Schematic of an industrial MHEX from Linde.[4]

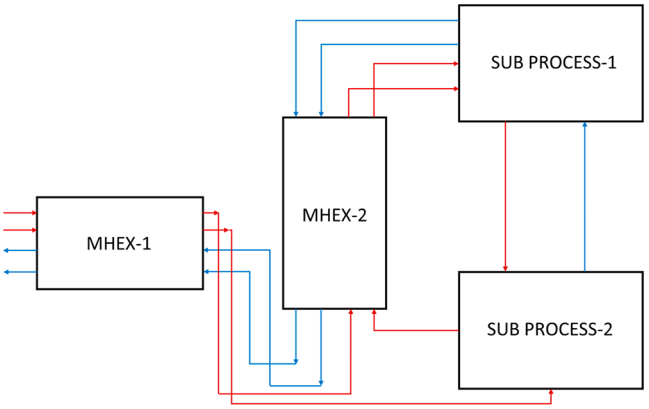

Figure 2. Schematic of a process with multiple MHEXs. The red lines represent hot streams, and the blue lines represent cold streams.

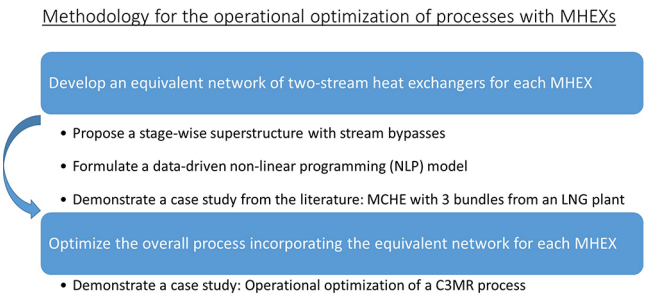

Figure 3. Methodology.

temperature approach during process optimization. They considered MHEXs as heat exchanger networks without utilities, used a disjunctive formulation to detect phases, and implemented simultaneous flowsheet optimization and heat integration. Following Kamath et al.,[5] Watson et al.[6] presented a nonsmooth simulation model for MHEXs also based on the pinch concept. Without considering phase changes, they revised the equation describing the pinch location and allowed up to three unknown variables to be computed simultaneously. Subsequently, Watson and Barton[7] extended their formulation[6] to model phase changes and nonideal thermodynamics. Employing the nonsmooth flowsheeting strategy developed by Watson et al.,[8] Vikse et al.[9] demonstrated the simulation of three single mixed refrigerant (SMR) processes for natural gas liquefaction. Then, Watson et al.[10] illustrated the optimization of SMR natural gas liquefaction processes using nondifferentiable models. Pattison and Baldea[11] proposed an equation-oriented model for MHEXs using a pseudotransient framework involving ordinary differential and algebraic equations (ODAEs). Tsay et al.[12] extended this model[11] to optimize processes while implicitly considering the detailed geometrical design of spiral-wound MHEXs. Similarly, Skaugen et al.[13] showed the design of an SMR process with a detailed plate and fin MHEX model that also includes geometric considerations.

Some studies have addressed process design considering MHEXs as a network of two-stream exchangers. Yee et al.[14] proposed a simultaneous heat integration model for area and energy targeting and discussed its application to design MHEXs. However, they considered constant heat capacities and ignored phase changes. In addition, they assumed isothermal mixing and did not consider pressure drops. Addressing the above limitations, Rao et al.[1] presented an equation-based model for MHEX design that ensures the feasibility of heat exchanges, enables simultaneous overall process optimization, and accommodates arbitrary and unknown phase changes of streams during the optimization process without using any Boolean variables.

In contrast to the above works, very few studies in the literature have developed predictive models for MHEXs, which precede system-wide operational optimization. Goyal et al.[15] and Skaugen et al.[16] reported geometry-specific models based on first-principles. While Goyal et al.[15] considered plate and fin MHEXs, Skaugen et al.[16] considered multiple types of MHEXs. However, in most cases, such geometry-dependent models are not feasible, as internal details of MHEXs are hardly available. Besides, first-principles predictive models are typically computation-intensive and hence, not desirable for process-wide optimization. Thus, simpler geometry-independent models that relate inputs to outputs are more favorable. However, very few such generic predictive models exist in the literature.

Hasan et al.[2] were the first to model the operation of an MHEX using a hypothetical network of two-stream heat exchangers. They proposed a mixed-integer nonlinear programming (MINLP) formulation using operational data for finding the best equivalent network representing an MHEX. Their formulation incorporated stream phase changes but allowed only one cold stream. They did not consider heat leaks and pressure drops common in an MHEX.

Khan et al.[17] developed an ANN (artificial neural network) model for MHEXs using simulated operational data. Jiang et al.[18] used a simple regression model to correlate the outlet temperatures of an MHEX in air separation units to its inlet temperatures and flows. Such predictive models may not do well when the training data are limited and the actual operation is away from the training conditions.[2] Besides, with no physical insights, they may not even ensure thermodynamic feasibility. Thus, there is a need to develop a reliable predictive model for MHEXs that addresses the above shortcomings.

In this work, we first discuss a generic predictive modeling approach for MHEXs based on historic operational data (Figure 3). Similar to Hasan et al.,[2] a network of two-stream

DOI: 10.1021/acs.iecr.8b05270
Ind. Eng. Chem. Res. 2019, 58, 5838−5850

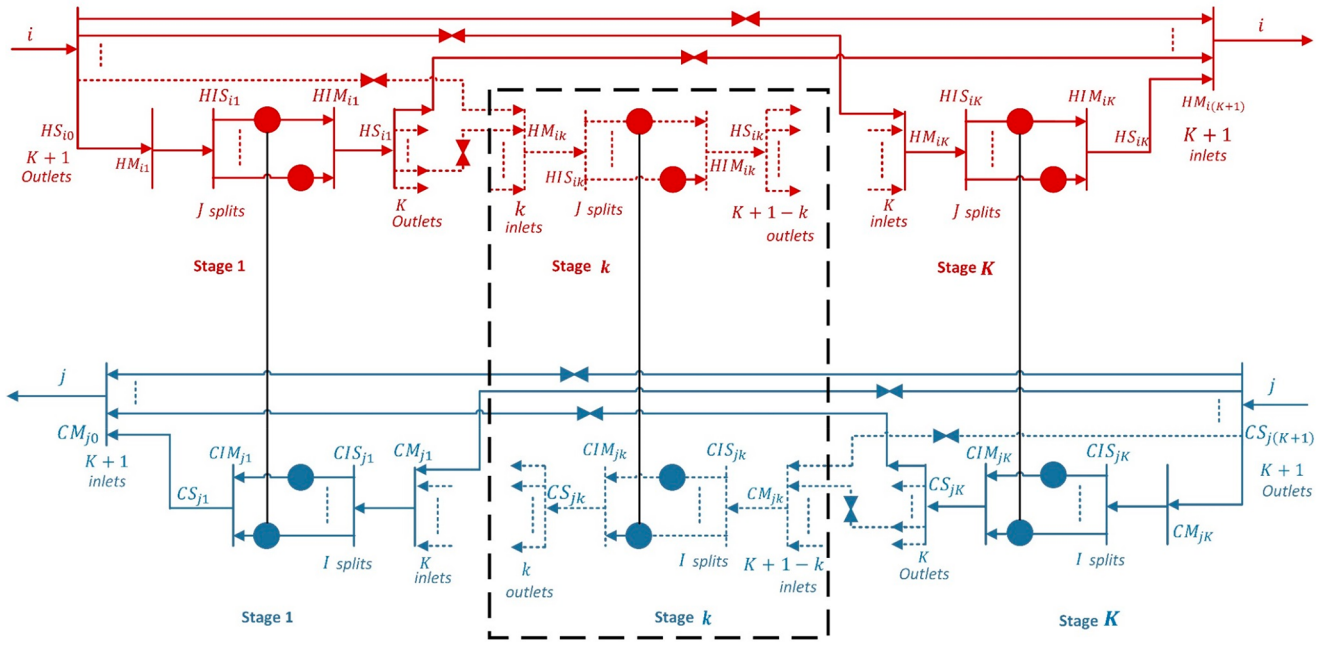

Figure 4. Schematic of the superstructure.

exchangers is used to represent the MHEX. Our formulation to synthesize the heat exchange network for an MHEX accommodates multiple hot and cold streams, ambient heat leak, and stream pressure drops. In addition, the formulation is applicable to any type of MHEX and has no binary variables, thus making it NLP rather than MINLP. We then apply our formulation on the LNG case study reported in Hasan et al.[2] Following this, we demonstrate the operational optimization of an example C3MR natural gas liquefaction process using our predictive model for its main cryogenic heat exchanger (MCHE). The methodology of this work is depicted in Figure 3.

PREDICTIVE MODEL FOR MULTISTREAM HEAT EXCHANGERS (MHEXs)

A typical MHEX involves multiple bundles. If we can develop a predictive model for each bundle, then we can model the entire MHEX. Therefore, consider the steady-state operation of a bundle in an existing MHEX. Let I hot streams ($i = 1, 2...I$) and J cold streams ($j = 1, 2...J$) pass through this bundle. N distinct steady-state data sets ($n = 1, 2, ..., N$), each with flows, compositions, and inlet−outlet conditions (i.e., temperature or enthalpy and pressure), of all exchanging streams are available. Using these data, we wish to synthesize a network of two-stream exchangers to best describe the bundle operation.

Assumptions:

(1) The bundle can be represented by a fixed network of two-stream exchangers with fixed areas. In other words, the connections among the fixed-area exchangers are also fixed and characteristic of the bundle.
(2) The composition of the exchanging streams does not vary significantly across all data sets. We consider average stream compositions across the data sets.
(3) All heat exchanges are counter-current.
(4) A hot process stream heats cold process streams only and vice versa. This assumption is justified, because like-streams usually flow in separate conduits with minimal interactions between them. For example, hot streams flow in separate sets of concentric tubes in a spiral-wound heat exchanger or through separate plates in a plate and fin heat exchanger.[2]

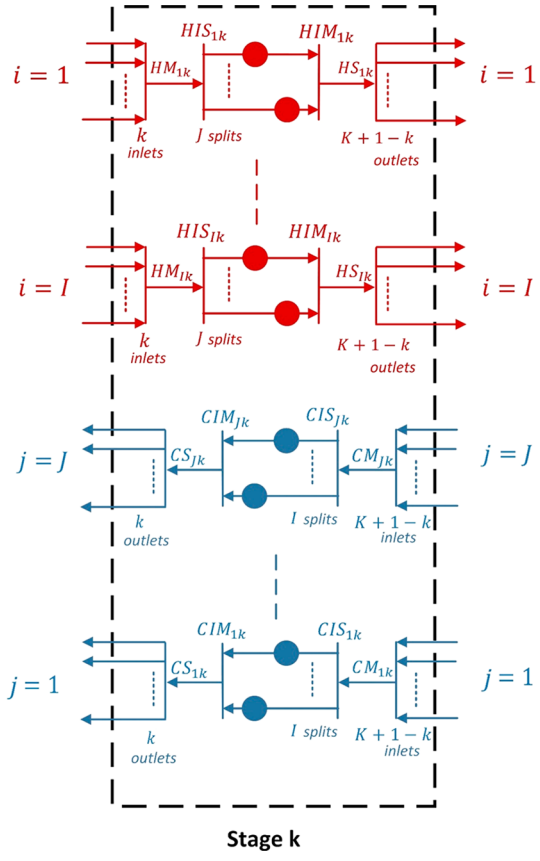

Figure 5. Stage k in the superstructure.

Superstructure for Heat Exchange Network. We represent the operation of the bundle by a network of simple two-stream heat exchangers. For finding this network, we

DOI: 10.1021/acs.iecr.8b05270
Ind. Eng. Chem. Res. 2019, 58, 5838−5850

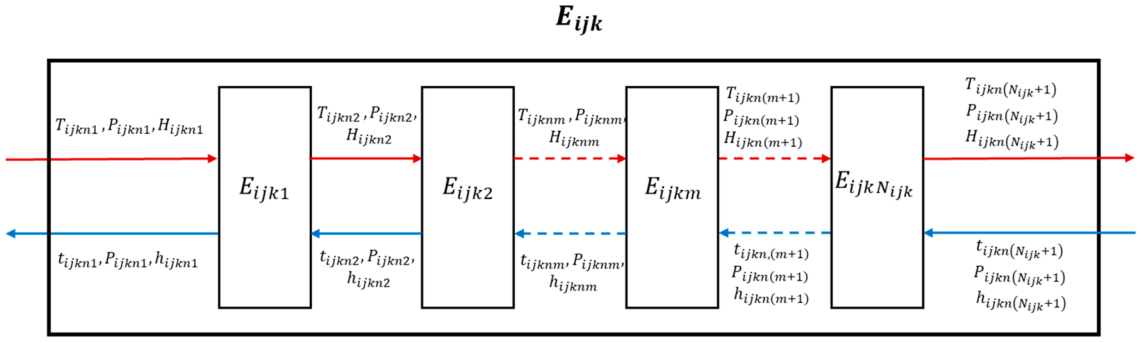

Figure 6. Segments within E_{ijk}

Table 1. Model Details

bundle		HB	MB	CB
no. of data sets	training		22	
	validation		6	
no. of streams	hot	4	4	2
	cold	1	1	1
no. of stages		1	2	1
no. of segments		3	1	3
solution times (s)	model M1	29	106	1.7
	model M2	961	182	41
	M2 only	failed	2853	1325
no. of equations	model M1	3475	3309	1883
	model M2	13 685	6655	6989
no. of variables	model M1	3641	3400	1999
	model M2	11 831	6842	6095

propose a superstructure (Figure 4) with $(K + 1)$ stages ($k = 0, 1, ..., K, K + 1$) for each stream. While a hot stream flows from its stage 0 to stage $(K + 1)$, a cold stream flows from its stage $(K + 1)$ to stage 0. Stage 0 of hot stream i has a splitter HS_{i0}, and stage $(K + 1)$ has a mixer $HM_{i(K+1)}$. In contrast, stage $(K + 1)$ of cold stream j has a splitter $CS_{j(K+1)}$, and stage 0 has a mixer CM_{j0}. Stages 1 through K of each stream permit heat exchange between the stream and all other eligible streams.

Each stage k ($k = 1, 2, ..., K$) consists of a stage mixer, an internal splitter, several parallel two-stream exchangers for the heat exchange, followed by an internal mixer, and finally a stage splitter (Figure 5). Thus, for hot stream i, its stage k ($1 \le k \le K$), comprises a stage mixer (HM_{ik}), which feeds the internal splitter (HIS_{ik}). HIS_{ik} produces J substreams, one for heating each cold stream j ($1 \le j \le J$) in a two-stream exchanger (E_{ijk}). The hot substreams from these J exchangers enter the internal mixer (HIM_{ik}) that feeds the stage splitter (HS_{ik}). For cold stream j, the corresponding entities are the stage mixer (CM_{jk}), internal splitter (CIS_{jk}), I two-stream exchangers (E_{ijk}, $1 \le i \le I$), internal mixer (CIM_{jk}), and stage splitter (CS_{jk}).

Figure 4 shows that HM_{ik} mixes k streams, one each from stages 0 to $k - 1$. CM_{jk} mixes $(K + 1 - k)$ streams, one each from stages $(K + 1)$ to $(k + 1)$. HS_{ik} produces $(K + 1 - k)$ substreams, one each for stages $(k + 1)$ to $(K + 1)$. CS_{jk} produces k streams, one each for stage k to 0. From Figure 5, we see that HIS_{ik} produces J substreams ($1 \le j \le J$) for E_{ijk}. CIS_{jk} produces I substreams ($1 \le i \le I$) for E_{ijk}. Finally, hot stream i exits the bundle from $HM_{i(K+1)}$, and cold stream j exits from CM_{j0}.

In contrast to other stagewise superstructures,[2,14,19] a stream from any stage can bypass one or more subsequent stages, which allows us to capture potential channeling that may exist in a bundle.

Formulation for Network Synthesis. Let s denote any stream (hot or cold) passing through the bundle. The following are defined for each data set n ($n = 1, 2, ..., N$).

F_{sn} ($s = i$ or j): Flow (mass or mol) of stream s.
TI_{sn}: Inlet temperature of stream s.
TO_{sn}: Outlet temperature of stream s.
PI_{sn}: Inlet pressure of stream s.
PO_{sn}: Outlet pressure of stream s.
HI_{sn}: Inlet specific enthalpy (J/kg or J/mol) of stream s.
HO_{sn}: Outlet specific enthalpy (J/kg or J/mol) of stream s.

The stream flows along the various connections in the network are governed by a set of split fractions (defined next), which characterize the flow distribution for each stream in the bundle. The split fractions for the stage splitters are

$x_{ikk'}$: Fraction of hot stream i flowing from HS_{ik} ($0 \le k \le K$) to $HM_{ik'}$ ($k + 1 \le k' \le K + 1$).

$$\sum_{k'=k+1}^{K+1} x_{ikk'} = 1 \qquad (1 \le i \le I;\ 0 \le k \le K) \tag{1a}$$

$y_{jkk'}$: Fraction of cold stream j flowing from CS_{ik} ($K + 1 \le k \le 1$) to $CM_{ik'}$ ($0 \le k' \le k - 1$).

$$\sum_{k'=0}^{k-1} y_{jkk'} = 1 \qquad (1 \le j \le J;\ 1 \le k \le K + 1) \tag{1b}$$

The split fractions for the internal splitters are

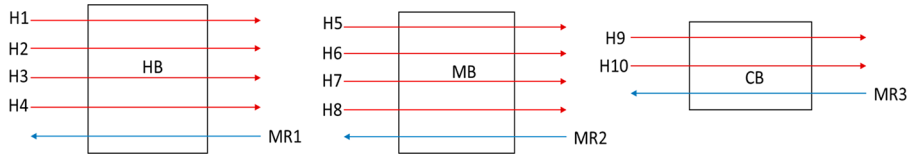

Figure 7. Schematic of the MCHE bundles in the LNG case study reported in Hasan et al.[2]

DOI: 10.1021/acs.iecr.8b05270
Ind. Eng. Chem. Res. 2019, 58, 5838−5850

Table 2. Regression Coefficients Used To Compute the Boundary Points

coefficients	H1, H5	H2, H6	H9	H4, H8	H3, H7, H10	MR1, MR2	MR3
$\beta_s^{GT} \times 10^2$	−0.0131	−0.036	−0.0397	−0.0117	−0.0086	−1.702	−0.5014
$\gamma_s^{GT} \times 10^2$	1.0938	3.396	2.1777	1.6491	1.0972	17.721	8.2105
$\delta_s^{GT} \times 10^2$	199.21	286.14	207.53	241.66	206.77	178.29	168.78
$\beta_s^{GH} \times 10^3$	−0.8761	−2.894	−1.3904	−1.0321	−0.5204	−21.961	−16.629
$\gamma_s^{GH} \times 10^3$	23.034	177.29	46.01	51.42	15.346	339.49	238.25
$\delta_s^{GH} \times 10^3$	−76451	−103169	−76713	−84920	−70974	−82982	−72025
$\beta_s^{LT} \times 10^2$	−0.0097	0.00	−0.0448	0.00	0.00	−1.374	−0.4559
$\gamma_s^{LT} \times 10^2$	1.8127	3.1832	3.1932	1.6993	1.104	15.848	8.3756
$\delta_s^{LT} \times 10^2$	128.42	179.73	115.88	155.1	130.65	75.392	81.271
$\beta_s^{LH} \times 10^3$	−0.0158	0.00	−2.2588	0.00	0.00	−29.107	−24.432
$\gamma_s^{LH} \times 10^3$	101.69	321.17	190.87	146.11	82.384	580.02	461.36
$\delta_s^{LH} \times 10^3$	−86879	−128740	−88760	−101868	−82936	−100632	−85299

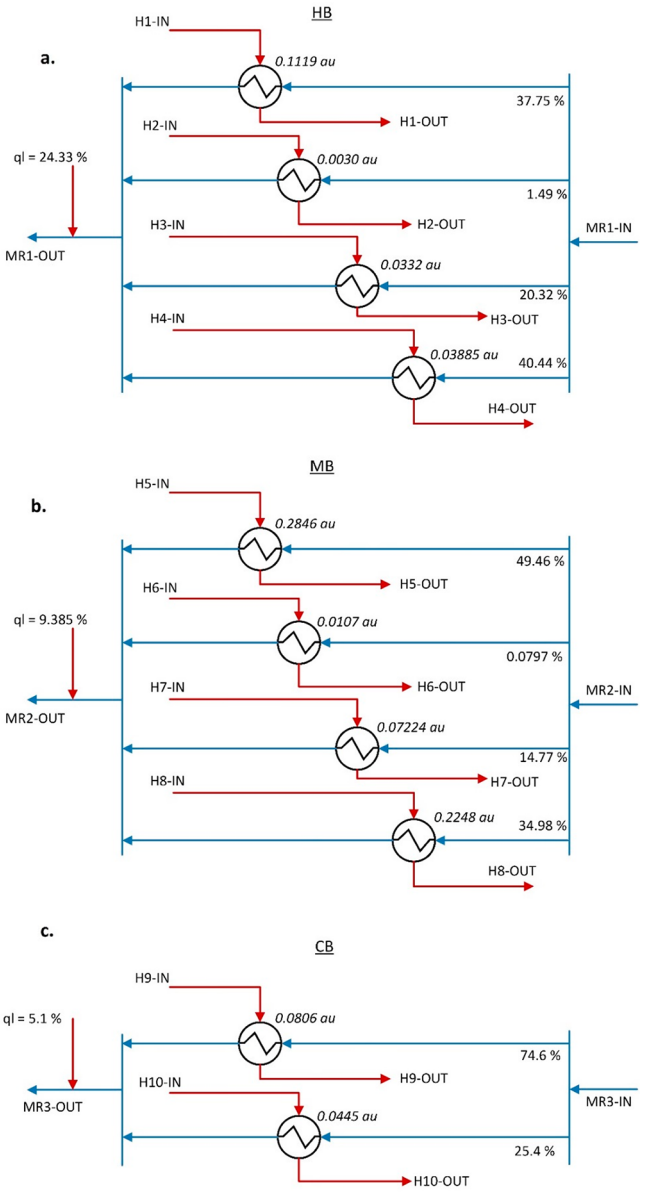

Figure 8. Equivalent two-stream exchanger networks for the MCHE bundles.

f_{ijk}: Fraction of hot stream i flowing from HIS_{ik} $(1 \le k \le K)$ to E_{ijk} $(1 \le j \le J)$.

$$\sum_j f_{ijk} = 1 \qquad (1 \le i \le I;\ 1 \le k \le K) \tag{2a}$$

g_{ijk}: Fraction of cold stream j flowing from CIS_{ik} $(1 \le k \le K)$ to E_{ijk} $(1 \le i \le I)$.

$$\sum_i g_{ijk} = 1 \qquad (1 \le j \le J;\ 1 \le k \le K) \tag{2b}$$

Our task now is to formulate an optimization problem that derives the best fixed-area heat exchanger network characterized by the above-mentioned fixed split fractions for each stream so as to explain the given N data sets of observed operation. To this end, we define the following for stage k of data set n $(n = 1, 2, ..., N)$.

FH_{ikn}: Flow (mass or mole) of hot stream i entering HS_{ik} $(0 \le k \le K,\ FH_{i0n} = F_{in})$
FC_{jkn}: Flow (mass or mole) of cold stream j entering CS_{jk} $(1 \le k \le K+1,\ FC_{j(K+1)n} = F_{jn})$
HSH_{ikn}: Specific enthalpy of hot stream i entering HS_{ik} $(0 \le k \le K,\ HSH_{i0n} = HI_{in})$
CSH_{jkn}: Specific enthalpy of cold stream j entering CS_{jk} $(1 \le k \le K+1,\ CSH_{j(K+1)n} = HI_{jn})$
HMH_{ikn}: Specific enthalpy of hot stream i exiting HM_{ik} $(1 \le k \le K+1)$
CMH_{jkn}: Specific enthalpy of cold stream j exiting CM_{jk} $(0 \le k \le K)$
$HOUT_{ijkn}$: Specific enthalpy of hot stream i exiting E_{ijk} $(1 \le k \le K)$
$COUT_{ijkn}$: Specific enthalpy of cold stream j exiting E_{ijk} $(1 \le k \le K)$
Q_{ijkn}: Heat exchange duty of E_{ijk} $(1 \le k \le K)$ for the data set n

Mass and energy balances across HM_{ik} and CM_{jk} give us

$$FH_{ikn} = \sum_{k'=0}^{k-1} FH_{ik'n}\, x_{ik'k} \qquad (1 \le i \le I;\ 1 \le k \le K+1) \tag{3a}$$

$$FH_{ikn}HMH_{ikn} = \sum_{k'=0}^{k-1} FH_{ik'n}\, x_{ik'k}\, HSH_{ik'n} \qquad (1 \le i \le I;\ 1 \le k \le K+1) \tag{3b}$$

$$FC_{jkn} = \sum_{k'=k+1}^{K+1} FC_{jk'n}\, y_{jk'k} \qquad (1 \le j \le J;\ 0 \le k \le K) \tag{4a}$$

DOI: 10.1021/acs.iecr.8b05270
Ind. Eng. Chem. Res. 2019, 58, 5838−5850

$$FC_{jkn}CMH_{jkn} = \sum_{k'=k+1}^{K+1} FC_{jk'n}\, y_{jk'k} CSH_{jk'n} \quad (1 \le j \le J;\ 0 \le k \le K) \tag{4b}$$

Likewise, mass and energy balances around HIM_{ik} and CIM_{jk} give us

$$HSH_{ikn} = \sum_{j} f_{ijk} HOUT_{ijkn} \qquad (1 \le i \le I;\ 1 \le k \le K) \tag{5}$$

$$CSH_{jkn} = \sum_{i} g_{ijk} COUT_{ijkn} \qquad (1 \le j \le J;\ 1 \le k \le K) \tag{6}$$

For E_{ijk} $(1 \le i \le I;\ 1 \le j \le J;\ 1 \le k \le K)$, we can write

$$HMH_{ikn} \ge HOUT_{ijkn} \tag{7}$$

$$COUT_{ijkn} \ge CMH_{jkn} \tag{8}$$

$$\begin{aligned} Q_{ijkn} &= f_{ijk} FH_{ikn}(HMH_{ikn} - HOUT_{ijkn}) \\ &= g_{ijk} FC_{jkn}(COUT_{ijkn} - CMH_{jkn}) \qquad (1 \le k \le K) \end{aligned} \tag{9}$$

Then, the heat duty of a stage for a stream s (SQ_{skn}) is given by

$$SQ_{ikn} = \sum_{j=1}^{J} Q_{ijkn} \tag{10}$$

$$SQ_{jkn} = \sum_{i=1}^{I} Q_{ijkn} \tag{11}$$

Now, we assume that the pressure drops across the bundle observed in the operational data are distributed among the heat exchange stages in proportion to their duties. For the data set n, let PIN_{ikn} $(PIN_{i1n} = PI_{in})$ and $POUT_{ikn}$ $(POUT_{iKn} = PO_{in})$ be the respective pressures of the hot stream i entering and exiting a stage k. Likewise, pin_{jkn} $(pin_{jKn} = PI_{jn})$ and $pout_{jkn}$ $(pout_{j1n} = PO_{jn})$ are the respective pressures of the cold stream j entering and exiting a stage k.

For any stream s, the inlet pressure of a stage is the outlet pressure of the previous stage.

$$PIN_{ijkn} = POUT_{i(k-1)n} \qquad (2 \le k \le K) \tag{12}$$

$$pin_{jkn} = pout_{j(k+1)n} \qquad (1 \le k \le K-1) \tag{13}$$

We distribute the pressure drops across stages in proportion to their heat duties using the following equations.

$$TQ_{sn} = \sum_{k=1}^{K} SQ_{skn} \tag{14}$$

$$(PIN_{ikn} - POUT_{ikn})TQ_{in} = SQ_{ikn}(PI_{in} - PO_{in}) \quad (1 \le k \le K) \tag{15}$$

$$(pin_{jkn} - pout_{jkn})TQ_{jn} = SQ_{jkn}(PI_{jn} - PO_{jn}) \quad (1 \le k \le K) \tag{16}$$

where, TQ_{sn} is the total heat duty of stream s for the entire bundle.

Let $\overline{HOUT}_{in}$ be the enthalpy of hot stream i exiting the bundle in data set n. Then,

$$\overline{HOUT}_{in} = HMH_{i(K+1)n} \tag{17}$$

The heat leak to or gain from the ambient environment is prominent in applications employing MHEXs. We assume that such losses or gains occur only at the end of the bundle for each cold stream. Hence, we add/remove a fraction $(qc_j \ge 0)$ of its total bundle duty to/from the enthalpy of each cold stream exiting the last stage.

$$\overline{COUT}_{jn} = [CMH_{j0n} \pm qc_j(CMH_{j0n} - HI_{jn})] \tag{18}$$

where, $\overline{COUT}_{jn}$ is the enthalpy of the cold stream j exiting the bundle. The above loss/gain must be decided specifically for each stream depending on its average temperature relative to the ambient.

Then, let MTA_{ij} be the minimum approach temperature desired between two exchanging streams i and j. To ensure thermodynamic feasibility at the end points of the bundle, we impose bounds on stream enthalpies as follows. Let $H_{ijn}^{\min}$ and $h_{ijn}^{\max}$ represent the lower and upper bounds for the exit enthalpies of the hot and cold streams, respectively. $H_{ijn}^{\min}$ is the specific enthalpy of hot stream i at $\min_j(TI_{jn} + MTA_{ij})$ and PO_{in}, and $h_{ijn}^{\max}$ is the specific enthalpy of cold stream j at $\max_i(TI_{in} - MTA_{ij})$ and PO_{jn}.

$$HMH_{i(K+1)n} \ge H_{ijn}^{\min} \tag{19}$$

$$CMH_{j0n} \le h_{ijn}^{\max} \tag{20}$$

Eqs 19 and 20 do not guarantee that the minimum temperature approach is respected throughout the bundle. Therefore, we divide each exchanger E_{ijk} $(i = 1, ..., I;\ j = 1, ..., J;\ k = 1, ..., K)$ into N_{ijk} prefixed segments $(E_{ijkm},\ m = 1, 2, \ldots N_{ijk})$ with equal heat duty (Figure 6) and impose temperature approach constraints at the ends of each segment. For this, let us define the following for each data set n:

H_{ijknm}: Specific enthalpy of hot stream i entering E_{ijkm}
h_{ijknm}: Specific enthalpy of cold stream j exiting E_{ijkm}
P_{ijknm}: Pressure of hot stream i entering E_{ijkm}
p_{ijknm}: Pressure of cold stream j exiting E_{ijkm}

We assume that the pressure drop across each segment in E_{ijk} is proportional to its heat duty. Consequently, each segment has the same pressure drop. Unless mentioned otherwise, all equations from here on are defined for stages $(1 \le k \le K)$ only.

As each segment within an E_{ijk} has the same duty, and hence, the same pressure drop, we write

$$H_{ijknm} = HMH_{ijkn} - \frac{(m-1)\cdot(HMH_{ijkn} - HOUT_{ijkn})}{N_{ijk}} \qquad (1 \le m \le N_{ijk} + 1) \tag{21a}$$

$$h_{ijknm} = COUT_{ijkn} - \frac{(m-1)\cdot(COUT_{ijkn} - CMH_{ijkn})}{N_{ijk}} \qquad (1 \le m \le N_{ijk} + 1) \tag{21b}$$

$$P_{ijknm} = PIN_{ijkn} - \frac{(m-1)(PIN_{ikn} - POUT_{ikn})}{N_{ijk}} \qquad (1 \le m \le N_{ijk} + 1) \tag{21c}$$

DOI: 10.1021/acs.iecr.8b05270
Ind. Eng. Chem. Res. 2019, 58, 5838−5850

$$p_{ijknm} = pout_{jkn} + \frac{(m-1)(pin_{jkn} - pout_{jkn})}{N_{ijk}} \quad (1 \le m \le N_{ijk} + 1) \tag{21d}$$

Now, to write proper minimum temperature approach constraints, we must correlate specific enthalpy (H) with stream temperature (T) and pressure (P). For a stream with fixed composition, H is a zone-dependent (subcooled, two-phase, superheated) function of (T, P) as follows

$$H(T, P) = \begin{cases} H_{SC}(T, P) & T \le BPT(P) \\ H_{TP}(T, P) & BPT(P) < T < DPT(P) \\ H_{SH}(T, P) & T \ge DPT(P) \end{cases} \tag{22}$$

where, $DPT(P)$ and $BPT(P)$ are the dew and bubble point temperatures of the stream. To compute $T(H, P)$, we must detect the zone of the stream at each segment. For this, let us define the following for each data set n.

T_{ijknm}: Temperature of hot stream i entering E_{ijkm}
t_{ijknm}: Temperature of cold stream j exiting E_{ijkm}
DPT_{ijknm}: Dew point temperature (DPT) of hot stream i entering E_{ijkm}
dpt_{ijknm}: Dew point temperature (DPT) of cold stream j exiting E_{ijkm}
BPT_{ijknm}: Bubble point temperature (BPT) of hot stream i entering E_{ijkm}
bpt_{ijknm}: Bubble point temperature (BPT) of cold stream j exiting E_{ijkm}
DPH_{ijknm}: Dew point enthalpy of hot stream i entering E_{ijkm}
dph_{ijknm}: Dew point enthalpy of cold stream j exiting E_{ijkm}
BPH_{ijknm}: Bubble point enthalpy of hot stream i entering E_{ijkm}
bph_{ijknm}: Bubble point enthalpy of cold stream j exiting E_{ijkm}

In this work, we express the specific enthalpy (H) for each stream as a function of stream temperature (T) and pressure (P) assuming an average composition. We now correlate BPTs and DPTs and corresponding specific enthalpies as quadratic functions of pressure. Eqs 23a−33 are defined for ($1 \le i \le I$; $1 \le j \le J$; $1 \le k \le K$; $1 \le n \le N$, $1 \le m \le N_{ijk} + 1$).

$$DPT_{ijknm} = \beta_i^{GT}(P_{ijknm})^2 + \gamma_i^{GT}P_{ijknm} + \delta_i^{GT} \tag{23a}$$

$$BPT_{ijknm} = \beta_i^{LT}(P_{ijknm})^2 + \gamma_i^{LT}P_{ijknm} + \delta_i^{LT} \tag{23b}$$

$$dpt_{ijknm} = \beta_j^{GT}(p_{ijknm})^2 + \gamma_j^{GT}p_{ijknm} + \delta_j^{GT} \tag{23c}$$

$$bpt_{ijknm} = \beta_j^{LT}(p_{ijknm})^2 + \gamma_j^{LT}p_{ijknm} + \delta_j^{LT} \tag{23d}$$

$$DPH_{ijknm} = \beta_i^{GH}(P_{ijknm})^2 + \gamma_i^{GH}P_{ijknm} + \delta_i^{GH} \tag{24a}$$

$$BPH_{ijknm} = \beta_i^{LH}(P_{ijknm})^2 + \gamma_i^{LH}P_{ijknm} + \delta_i^{LH} \tag{24b}$$

$$dph_{ijknm} = \beta_j^{GH}(p_{ijknm})^2 + \gamma_j^{GH}p_{ijknm} + \delta_j^{GH} \tag{24c}$$

$$bph_{ijknm} = \beta_j^{LH}(p_{ijknm})^2 + \gamma_j^{LH}p_{ijknm} + \delta_j^{LH} \tag{24d}$$

The coefficients in eqs 23a−24d are estimated by regressing these properties from a simulator such as Aspen Hysys.

Next, let T_{ijknm}^{SH}, T_{ijknm}^{TP}, T_{ijknm}^{SC} be the temperatures of hot stream i entering E_{ijkm} if it were in the superheated, two-phase, or subcooled zones, respectively. Similarly, let t_{ijknm}^{SH}, t_{ijknm}^{TP}, t_{ijknm}^{SC} be the respective temperatures for cold stream j exiting E_{ijkm}. Then, let the following define the departures of the above-mentioned temperatures from their respective zone boundaries (DPT and BPT).

$$\Delta T_{ijknm}^{SH} = T_{ijknm}^{SH} - DPT_{ijknm} \tag{25a}$$

$$\Delta T_{ijknm}^{TP} = DPT_{ijknm} - T_{ijknm}^{TP} \tag{25b}$$

$$\Delta T_{ijknm}^{SC} = BPT_{ijknm} - T_{ijknm}^{SC} \tag{25c}$$

$$\Delta t_{ijknm}^{SH} = t_{ijknm}^{SH} - dpt_{ijknm} \tag{25d}$$

$$\Delta t_{ijknm}^{TP} = dpt_{ijknm} - t_{ijknm}^{TP} \tag{25e}$$

$$\Delta t_{ijknm}^{SC} = bpt_{ijknm} - t_{ijknm}^{SC} \tag{25f}$$

The enthalpy differences analogous to the above are

$$\Delta H_{ijknm}^{SH} = H_{ijknm} - DPH_{ijknm} \tag{26a}$$

$$\Delta H_{ijknm}^{TP} = DPH_{ijknm} - H_{ijknm} \tag{26b}$$

$$\Delta H_{ijknm}^{SC} = BPH_{ijknm} - H_{ijknm} \tag{26c}$$

$$\Delta h_{ijknm}^{SH} = h_{ijknm} - dph_{ijknm} \tag{26d}$$

$$\Delta h_{ijknm}^{TP} = dph_{ijknm} - h_{ijknm} \tag{26e}$$

$$\Delta h_{ijknm}^{SC} = bph_{ijknm} - h_{ijknm} \tag{26f}$$

Next, we define the following 0−1 continuous variables to detect zones.

$$z_{ijknm}^{SH} = \begin{cases} 1 & H_{ijknm} \ge DPH_{ijknm} \\ 0 & otherwise \end{cases}$$

$$z_{ijknm}^{SC} = \begin{cases} 1 & H_{ijknm} \le BPH_{ijknm} \\ 0 & otherwise \end{cases}$$

$$y_{ijknm}^{SH} = \begin{cases} 1 & h_{ijknm} \ge dph_{ijknm} \\ 0 & otherwise \end{cases}$$

$$y_{ijknm}^{SC} = \begin{cases} 1 & h_{ijknm} \le bph_{ijknm} \\ 0 & otherwise \end{cases}$$

We achieve the binary-like behavior of z_{ijknm}^{SH} by using the following constraints.

$$\Delta H_{ijknm}^{SH} z_{ijknm}^{SH} \ge 0 \tag{27a}$$

$$\Delta H_{ijknm}^{SH}(1 - z_{ijknm}^{SH}) \le 0 \tag{27b}$$

$$1 - z_{ijknm}^{SH} \le \Delta H_{ijknm}^{SH}(2z_{ijknm}^{SH} - 1)M \tag{27c}$$

If $\Delta H_{ijknm}^{SH} > 0$, then $z_{ijknm}^{SH} = 1$ to satisfy eq 27b. If $\Delta H_{ijknm}^{SH} < 0$, then $z_{ijknm}^{SH} = 0$ to satisfy eq 27a. If $\Delta H_{ijknm}^{SH} = 0$, then eq 27c forces $z_{ijknm}^{SH} = 1$. Clearly, the choice of M must ensure $|\Delta H_{ijknm}^{SH}| M \ge 1$ for sufficiently low values of $|\Delta H_{ijknm}^{SH}|$. Following the

DOI: 10.1021/acs.iecr.8b05270
Ind. Eng. Chem. Res. 2019, 58, 5838−5850

same arguments, we write eqs 28a−30c for other three variables.

$$\Delta H^{SC}_{ijknm} z^{SC}_{ijknm} \geq 0 \tag{28a}$$

$$\Delta H^{SC}_{ijknm}(1 - z^{SC}_{ijknm}) \leq 0 \tag{28b}$$

$$1 - z^{SC}_{ijknm} \leq \Delta H^{SC}_{ijknm}(2z^{SC}_{ijknm} - 1)M \tag{28c}$$

$$\Delta h^{SH}_{ijknm} y^{SH}_{ijknm} \geq 0 \tag{29a}$$

$$\Delta h^{SH}_{ijknm}(1 - y^{SH}_{ijknm}) \leq 0 \tag{29b}$$

$$1 - y^{SH}_{ijknm} \leq \Delta h^{SH}_{ijknm}(2y^{SH}_{ijknm} - 1)M \tag{29c}$$

$$\Delta h^{SC}_{ijknm} y^{SC}_{ijknm} \geq 0 \tag{30a}$$

$$\Delta h^{SC}_{ijknm}(1 - y^{SC}_{ijknm}) \leq 0 \tag{30b}$$

$$1 - y^{SC}_{ijknm} \leq \Delta h^{SC}_{ijknm}(2y^{SC}_{ijknm} - 1)M \tag{30c}$$

While previous studies[2,20] related the departure of specific enthalpy from the boundary point as a cubic function of the corresponding departure of temperature in each zone separately, we also include a linear dependence on stream pressure. We now propose the following zone-dependent cubic correlations for (a) non-negative ΔH^{SH}_{ijknm} and ΔT^{SH}_{ijknm}, (b) non-negative ΔH^{TP}_{ijknm} and ΔT^{TP}_{ijknm}, and (c) non-negative ΔH^{SC}_{ijknm} and ΔT^{SC}_{ijknm} in eqs 31a−31f.

$$\Delta H^{SH}_{ijknm} \cdot z^{SH}_{ijknm} = Cp_i^{SH}(1 + a_i^{SH} P_{ijknm}) \begin{pmatrix} \Delta T^{SH}_{ijknm} + b_i^{SH}(\Delta T^{SH}_{ijknm})^2 \\ + c_i^{SH}(\Delta T^{SH}_{ijknm})^3 \end{pmatrix} \tag{31a}$$

$$\Delta H^{TP}_{ijknm} \cdot (1 - z^{SH}_{ijknm} - z^{SC}_{ijknm}) = Cp_i^{TP}(1 + a_i^{TP} P_{ijknm}) \begin{pmatrix} \Delta T^{TP}_{ijknm} + b_i^{TP}(\Delta T^{TP}_{ijknm})^2 \\ + c_i^{TP}(\Delta T^{TP}_{ijknm})^3 \end{pmatrix} \tag{31b}$$

$$\Delta H^{SC}_{ijknm} \cdot z^{SC}_{ijknm} = Cp_i^{SC}(1 + a_i^{SC} P_{ijknm}) \begin{pmatrix} \Delta T^{SC}_{ijknm} + b_i^{SC}(\Delta T^{SC}_{ijknm})^2 \\ + c_i^{SC}(\Delta T^{SC}_{ijknm})^3 \end{pmatrix} \tag{31c}$$

$$\Delta h^{SH}_{ijknm} \cdot y^{SH}_{ijknm} = Cp_j^{SH}(1 + a_j^{SH} p_{ijknm}) \begin{pmatrix} \Delta t^{SH}_{ijknm} + b_j^{SH}(\Delta t^{SH}_{ijknm})^2 \\ + c_j^{SH}(\Delta t^{SH}_{ijknm})^3 \end{pmatrix} \tag{31d}$$

$$\Delta h^{TP}_{ijknm} \cdot (1 - y^{SH}_{ijknm} - y^{SC}_{ijknm}) = Cp_j^{TP}(1 + a_j^{TP} p_{ijknm}) \begin{pmatrix} \Delta t^{TP}_{ijknm} + b_j^{TP}(\Delta t^{TP}_{ijknm})^2 \\ + c_j^{TP}(\Delta t^{TP}_{ijknm})^3 \end{pmatrix} \tag{31e}$$

$$\Delta h^{SC}_{ijknm} \cdot y^{SC}_{ijknm} = Cp_j^{SC}(1 + a_j^{SC} p_{ijknm}) \begin{pmatrix} \Delta t^{SC}_{ijknm} + b_j^{SC}(\Delta t^{SC}_{ijknm})^2 \\ + c_j^{SC}(\Delta t^{SC}_{ijknm})^3 \end{pmatrix} \tag{31f}$$

We then pick the actual stream temperatures (T_{ijknm} and t_{ijknm}) from the above computed superheated (T^{SH}_{ijknm} and t^{SH}_{ijknm}), two-phase (T^{TP}_{ijknm} and t^{TP}_{ijknm}), and subcooled (T^{SC}_{ijknm} and t^{SC}_{ijknm}) zone temperatures as follows.

$$T_{ijknm} = T^{SH}_{ijknm} z^{SH}_{ijknm} + T^{TP}_{ijknm}(1 - z^{SH}_{ijknm} - z^{SC}_{ijknm}) + T^{SC}_{ijknm} z^{SC}_{ijknm} \tag{32a}$$

$$t_{ijknm} = t^{SH}_{ijknm} y^{SH}_{ijknm} + t^{TP}_{ijknm}(1 - y^{SH}_{ijknm} - y^{SC}_{ijknm}) + t^{SC}_{ijknm} y^{SC}_{ijknm} \tag{32b}$$

With this, we can ensure the thermodynamic feasibility of heat transfer in each segment as follows (Figure 6).

$$T_{ijknm} - t_{ijknm} \geq MTA_{ij} \qquad (1 \leq m \leq N_{ijk} + 1) \tag{33}$$

The arithmetic mean of the temperature differences across a segment is given by

$$AMTD_{ijknm} = \frac{\Delta T_{ijknm} + \Delta T_{ijkn(m+1)}}{2} \qquad 1 \leq m \leq N_{ijk} \tag{34}$$

where, $\Delta T_{ijknm} = T_{ijknm} - t_{ijknm}$.

In this work, we provide the correlations suitable for spiral-wound heat exchangers to estimate heat-transfer coefficients (HTC). We assume that hot streams flow in tubes, while cold streams flow in the shell. However, the approach is generic and can also be applied to any other class of MHEXs with other forms of correlations to compute HTCs. Following Hasan et al.,[2] we use the following correlation to estimate the heat-transfer coefficient h^t_{in} for hot streams

$$h^t_{in} = \alpha^t_i (F_{in})^{0.8} \tag{35}$$

where, α^t_i depends on the fluid and exchanger properties. Likewise, we use the following correlation to estimate the heat-transfer coefficient h^s_{jn} for cold streams

$$h^s_{jn} = \alpha^s_j (F_{jn})^{0.25} \tag{36}$$

where, α^t_i depends on the fluid and exchanger properties. With these, we compute the overall heat-transfer coefficient U_{ijn} for E_{ijkm} as follows

$$U_{ijn} = \frac{h^t_{in} \cdot h^s_{jn}}{h^t_{in} + h^s_{jn}} \tag{37}$$

Then, the heat-transfer area A_{ijknm} for E_{ijkm} is given by

$$A_{ijknm} = \frac{Q_{ijkn}}{U_{ijn} AMTD_{ijknm} N_{ijk}} \qquad 1 \leq m \leq N_{ijk} \tag{38}$$

We use the arithmetic mean temperature difference (AMTD) instead of the conventional log mean temperature difference (LMTD) in eq 38 for reducing nonlinearities and avoiding numerical difficulties associated with the latter. Exact LMTD calculation poses numerical difficulties when the temperature approaches for a segment are equal. Alternatively, the LMTD approximations from Chen[21] or Paterson[22] may be used.

Finally, our objective is to match the N sets of operational data with maximum accuracy. To this end, we minimize the sum of squares of the differences in observed and predicted exit stream enthalpies from the bundle.

$$\text{min.} \left\{ \sqrt{\sum_n \left[\sum_i (HO_{in} - \overline{HOUT_{in}})^2 + \sum_j (HO_{jn} - \overline{COUT_{jn}})^2 \right]} \right. \tag{39}$$

In addition, as we aim to estimate unique values of heat-transfer areas (A_{ijk}) for all exchangers, we also minimize the

DOI: 10.1021/acs.iecr.8b05270
Ind. Eng. Chem. Res. 2019, 58, 5838−5850

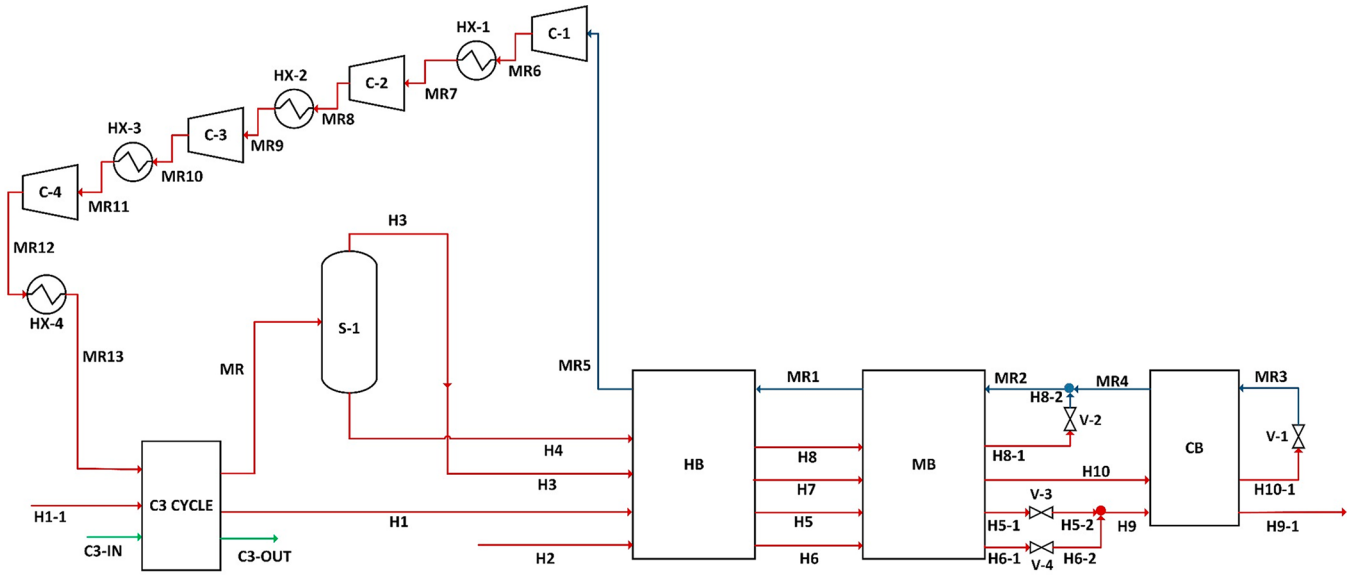

Figure 9. Simplified C3MR process with a three-bundle MCHE.

differences in the predicted areas A_{ijk} and the observed areas ($\sum_{m=1}^{N_{ijk}} A_{ijknm}$) of E_{ijk} in the data sets. Hence, the cumulative objective function for our NLP is as follows.

$$\text{min.} \left\{ \sqrt{\sum_n \left[\sum_i (HO_{in} - \overline{\overline{HOUT_{in}}})^2 + \sum_j (HO_{jn} - \overline{\overline{COUT_{jn}}})^2 \right]} + \sqrt{\sum_i \sum_j \sum_k \sum_n \left(A_{ijk} - \sum_{m=1}^{N_{ijk}} A_{ijknm} \right)^2} \right. \tag{40}$$

Let us refer to eqs 1a−20 and 39 as model 1 (M1) and eqs 1a−21d, 23a−38, and 40 as model 2 (M2).

Solution Strategy. First, we solve the simple model M1 that estimates the flow distribution ensuring minimum approach only at the ends of the bundle. The solution of M1 is then used to initialize the full model M2 that detects the zones traversed by the exchanging streams, ensures minimum approach throughout the bundle, and computes the heat-transfer areas of the exchangers in the network. We implemented these models in GAMS 24.6.1\BARON in a 64-bit Windows 7 desktop with a 3.6 GHz Intel Core i7 processor and 16 GB of RAM. The solution times for M1−M2 applied to the following case study is provided in Table 1. Without the initialization by M1, M2 alone could not be solved for one case (namely HB, as we see later). For other cases (MB and CB), the solution times (Table 1) were much longer without M1, but we obtained the same solutions.

LNG Case Study. We applied our models M1−M2 on the LNG case study reported in Hasan et al.[2]

As shown in Figure 7, the main cryogenic heat exchanger (MCHE) of an existing LNG plant consists of three bundles, viz. HB, MB, and CB. HB has four hot streams (H1, H2, H3, H4) and one cold stream (MR1). MB also has four hot streams (H5, H6, H7, H8) and one cold stream (MR2). CB has two hot streams (H9 and H10) and one cold stream (MR3). A total of 28 sets of operational data (scaled for confidentiality) for the bundles is presented in Hasan et al.[2] Table 1 provides the model details. Table 2 lists the regression coefficients for eqs 23a−23d and 24a−24d. We choose the number of heat exchange stages (K) for a bundle based on its heat load and the extent of phase change while also considering the complexity that an additional stage adds. Starting with a few stages, we choose the least K that gives an acceptable prediction error.

The network of two-stream heat exchangers that best represent the operation of these bundles is shown in Figure 8. Note that the network shown in Figure 8 is much simpler than that of Hasan et al.[2]

HB. For HB, we fixed the number of stages K = 1 and number of segments N_{ijk} = 3. We find that 37.75% of the MR1 cools H1 in $A^{HB}_{H1,MR1}$ = 0.1119 au of heat-transfer area, while 40.44% of MR1 cools H4 in $A^{HB}_{H4,MR1}$ = 0.03885 au of area. As the flow of H2 is low, only 1.49% of the MR1 cools H2 in $A^{HB}_{H2,MR1}$ = 0.002996 au of area. Then, 20.32% MR1 cools H3 in $A^{HB}_{H3,MR1}$ = 0.03318 au of area. MR1 exiting the last stage is added with an additional Ql^{HB} = 24.33% of the bundle heat duty to account for the ambient heat leak.

MB. It is clear from the operational data[2] that MB has the highest heat load. Hence, we fixed the number of stages K = 2 and number of segments N_{ijk} = 1. However, one of the stages disappeared in the model results. Hence, a single stage network of two-stream exchangers best represents the MB operation. We find that 49.46% of MR2 contacts H5 in $A^{MB}_{H5,MR2}$ = 0.2876 au of heat-transfer area. Only 0.0797% of MR2 cools H6 in $A^{MB}_{H6,MR2}$ = 0.01069 au of area. Next, 14.77% of the MR2 exchanges heat with H7 in $A^{MB}_{H7,MR2}$ = 0.07224 au of area. Lastly, 34.98% of the MR2 contacts H8 in $A^{MB}_{H8,MR2}$ = 0.2248 au of area. In addition, MR2 is added with Ql^{MB} = 9.385% of the bundle heat duty.

CB. In this case, we fixed the number of stages K = 1 and number of segments N_{ijk} = 3. H9 is cooled by 74.6% of MR3 in $A^{CB}_{H9,MR3}$ = 0.0806 au of area. Then, H10 is cooled by the rest of MR3 (25.4%) MR3 in $A^{CB}_{H10,MR3}$ = 0.0445 au of area. Finally, MR3 is added with Ql^{CB} = 5.1% of the bundle heat duty. Interestingly, the flow distribution for the CB discussed above exactly matches with that of Hasan et al.[2]

Model Prediction. The performance of the simple predictive model for the three bundles was evaluated on independent test sets of data.[2] Given the inlet conditions of the

DOI: 10.1021/acs.iecr.8b05270
Ind. Eng. Chem. Res. 2019, 58, 5838−5850

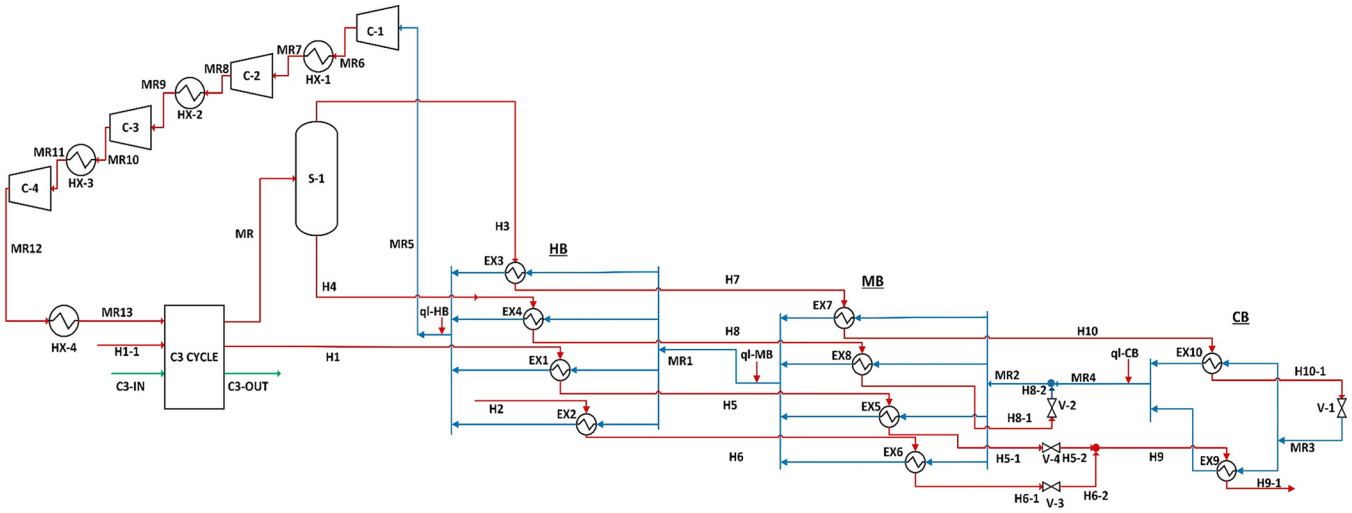

Figure 10. C3MR process with our predictive models for the MCHE.

Table 3. C3MR Optimization Details

problem details			our results[a]
objective function	min. $W_{C-1} + W_{C-2} + W_{C-3} + W_{C-4}$ (total compression power)		W_{C-1} = 3.756 qu
			W_{C-2} = 1.562 qu
			W_{C-3} = 1.141 qu
			W_{C-4} = 1.138 qu
decision variables	PR_{C-1}	pressure ratio of compressor-1	3.820
	PR_{C-2}	pressure ratio of compressor-2	1.648
	PR_{C-3}	pressure ratio of compressor-3	1.473
	PR_{C-4}	pressure ratio of compressor-4	1.509
	P_{MR3}	MR3 pressure	3.635 pu
	F_{MR}	MR molar flow rate	3.453 pu
	T_{MR}	MR temperature	2.336 tu
	T_{H1}	H1 temperature	2.338 tu
	T_{MR1}	MR1 temperature	2.089 tu
constraints	$\min(MTA_{EX1} + MTA_{EX2} + MTA_{EX3} + MTA_{EX4} + MTA_{EX5} + MTA_{EX6} + MTA_{EX7} + MTA_{EX8} + MTA_{EX9} + MTA_{EX10}) \geq 2$ °C; (Respect minimum approach temperature in all heat exchangers = 1.23 tu)		minimum approach temperature = 2.001 °C
	$T_{H9-1} \leq T^{max}_{H9-1}$; (H9−1 temperature must not exceed T^{max}_{H9-1})		
	vf_{MR5} = 1; (C-1 feed has a vapor fraction of 1)		
	vf_{MR7} = 1; (C-2 feed has a vapor fraction of 1)		
	vf_{MR9} = 1; (C-3 feed has a vapor fraction of 1)		
	vf_{MR11} = 1; (C-4 feed has a vapor fraction of 1)		

[a]qu: scaled power unit; pu: scaled pressure unit; fu: scaled molar flow unit; tu: scaled temperature unit.

exchanging streams and their pressure drops, our model for HB, MB, and CB predicted the outlet temperatures with maximum errors of 4.91, 6.46, and 4.65% respectively. Hence, this predictive model can be very useful to the plant operators to reduce the guesswork involved in the plant operation due to varying feed/ambient conditions.

OPERATIONAL OPTIMIZATION OF C3MR LIQUEFACTION PROCESS

We now demonstrate the operational optimization of a process employing MHEXs. The predictive models for the bundles of the MCHE discussed above can be conveniently incorporated within optimization routines to improve process operation. We consider an example C3MR natural gas liquefaction process (modified version of Wang et al.[23]) incorporating our predictive model for its main cryogenic heat exchanger (MCHE). As shown in Figure 9, the modified C3MR cycle has a simplified the propane cycle, an MCHE with three bundles and four stages of compression (75% adiabatic efficiency) with intercoolers.

Now, let us replace the MCHE in this case study by our predictive models for HB, MB, and CB as shown in Figure 10. Each exchanger in our predictive model has specified pressure drops. We then minimize the total compression work of the process respecting a minimum approach temperature in all the exchangers, maximum exit temperature for H9−1, and ensuring a superheated feed to all compressors (Table 3).

The exchangers of our predictive models for HB, MB, and CB along with other components of the C3MR are simulated in Aspen Hysys with the Peng−Robinson fluid package. With known heat-transfer areas (A) and correlations for heat-transfer coefficients (eqs 35−38), the values of their product (UA) for all the exchangers in our predictive models are specified. We then minimize the total compression work of the

DOI: 10.1021/acs.iecr.8b05270
Ind. Eng. Chem. Res. 2019, 58, 5838−5850

process with nine decision variables (Table 3) using the genetic algorithm in Matlab 2015a (interfaced with Hysys).

CONCLUSIONS

We proposed a procedure for the operational optimization of processes with multistream heat exchangers (MHEXs). The first step of the procedure is to develop a geometry-independent predictive model for each MHEX in the process using historical operational data. The predictive models are then used inside the overall process optimization problem.

Our predictive modeling approach involves synthesizing an equivalent network of simple two-stream heat exchangers that best represents the operation of an MHEX bundle. For finding this network, we proposed a stagewise superstructure that allows a stream from any stage to bypass one or more subsequent stages. Our nonlinear programming (NLP) formulation to synthesize the network handles multiple hot and cold streams, considers stream pressure drops, and includes ambient heat leak/gain.

We developed predictive models for the three bundles of the main cryogenic heat exchanger (MCHE) in an LNG plant[2] case study with a maximum error of 6.46%. Lastly, we demonstrated the operational optimization of an example C3MR natural gas liquefaction process incorporating our predictive models for the main cryogenic heat exchanger (MCHE).

AUTHOR INFORMATION

Corresponding Author

*E-mail: cheiak@nus.edu.sg.

ORCID

Iftekhar A. Karimi: 0000-0001-7122-0578

Notes

The authors declare no competing financial interest.

ACKNOWLEDGMENTS

This work was funded by the National University of Singapore through a seed grant (R261-508-001-646/733) for CENGas (Center of Excellence for Natural Gas). We thank AspenTech Inc. for the use of Aspen Hysys under academic licenses provided to the National University of Singapore.

NOTATIONS

Indices

s = Streams passing through a bundle
i = Hot streams passing through a bundle
j = Cold streams passing through a bundle
k = Stages in the superstructure
n = Data set
m = Segments in a heat exchanger

Abbreviations

AMTD = Arithmetic mean temperature difference
BPT = Bubble point temperature
DPT = Dew point temperature
HENS = Heat exchanger network synthesis
HTC = Heat-transfer coefficient
LMTD = Log mean temperature difference
LNG = Liquified natural gas
MCHE = Main cryogenic heat exchanger
MHEX = Multistream heat exchanger
MINLP = Mixed-integer nonlinear programming
NG = Natural gas
NLP = Nonlinear programming
SMR = Single mixed refrigerant

Parameters

F_{sn} = Molar flow of stream s in the MHEX bundle for data set n
TI_{sn} = Inlet temperature of stream s in the bundle for data set n
TO_{sn} = Outlet temperature of stream s in the bundle for data set n
PI_{sn} = Inlet pressure of stream s in the bundle for data set n
PO_{sn} = Outlet pressure of stream s in the bundle for data set n
HI_{sn} = Specific enthalpy of stream s entering the bundle for data set n
HO_{sn} = Specific enthalpy of stream s exiting the bundle for data set n
β_s^{GT}, γ_s^{GT}, δ_s^{GT} = Coefficients used to compute the dew point temperature of stream s
β_s^{LT}, γ_s^{LT}, δ_s^{LT} = Coefficients used to compute the bubble point temperature of stream s
β_s^{GH}, γ_s^{GH}, δ_s^{GH} = Coefficients used to compute the dew point enthalpy of stream s
β_s^{LH}, γ_s^{LH}, δ_s^{LH} = Coefficients used to compute the bubble point enthalpy of stream s
Cp_s^{SH}, a_s^{SH}, b_s^{SH}, c_s^{SH} = Coefficients used in the property correlations (specific enthalpy with temperature and pressure) of stream s in the superheated zone
Cp_s^{TP}, a_s^{TP}, b_s^{TP}, c_s^{TP} = Coefficients used in the property correlations of stream s in the two-phase zone
Cp_s^{SC}, a_s^{SC}, b_s^{SC}, c_s^{SC} = Coefficients used in the property correlations of stream s in the subcooled zone
α_i^t, α_j^s = Coefficients used to compute the tube and shell side HTCs
N_{ijk} = Number of segments in heat exchanger E_{ijk}
MTA_{ij} = Minimum approach temperature expected between a hot stream i and cold stream j
$H_{ijn}^{\min}$ = Lower bound on the enthalpy of the hot stream i exiting the bundle in data set n
$h_{ijn}^{\max}$ = Upper bound on the enthalpy of the cold stream j exiting the bundle in data set n

Variables

FH_{ikn} = Flow (mass or mole) of hot stream i entering HS_{ik}
FC_{jkn} = Flow (mass or mole) of cold stream j entering CS_{jk}
HSH_{ikn} = Specific enthalpy of hot stream i entering HS_{ik}
CSH_{jkn} = Specific enthalpy of cold stream j entering CS_{jk}
HMH_{ikn} = Specific enthalpy of hot stream i exiting HM_{ik}
CMH_{jkn} = Specific enthalpy of cold stream j exiting CM_{jk}
$HOUT_{ijkn}$ = Specific enthalpy of hot stream i exiting E_{ijk}
$COUT_{ijkn}$ = Specific enthalpy of cold stream j exiting E_{ijk}
Q_{ijkn} = Heat exchange duty of E_{ijk} for data set n
SQ_{skn} = Heat duty of stream s in stage k for data set n
PIN_{ikn} = Pressure of hot stream i entering HM_{ik}
$POUT_{ikn}$ = Pressure of hot stream i exiting HS_{ik}
$pout_{jkn}$ = Pressure of cold stream j entering CM_{jk}
$pout_{jkn}$ = Pressure of cold stream j exiting CS_{jk}
TQ_{sn} = Total heat duty of stream s in the bundle in data set n
qc_j = Fraction of the total bundle duty of stream j to account for the ambient heat leak/gain
f_{ijk} = Fraction of hot stream i flowing from HIS_{ik} to E_{ijk}
g_{ijk} = Fraction of cold stream j flowing from CIS_{ik} to E_{ijk}

DOI: 10.1021/acs.iecr.8b05270
Ind. Eng. Chem. Res. 2019, 58, 5838−5850

$x_{ikk'}$ = Fraction of hot stream i flowing from HS_{ik} to $HM_{ik'}$
$y_{jkk'}$ = Fraction of cold stream j flowing from CS_{ik} to $CM_{ik'}$
$\overline{\overline{HOUT}}_{in}$ = Specific enthalpy of the hot stream i exiting the bundle in data set n
$\overline{\overline{COUT}}_{jn}$ = Specific enthalpy of the cold stream j exiting the bundle in data set n
H_{ijknm} = Specific enthalpy of hot stream i entering E_{ijkm}
h_{ijknm} = Specific enthalpy of cold stream j exiting E_{ijkm}
P_{ijknm} = Pressure of hot stream i entering E_{ijkm}
p_{ijknm} = Pressure of cold stream j exiting E_{ijkm}
T_{ijknm} = Temperature of hot stream i entering E_{ijkm}
t_{ijknm} = Temperature of cold stream j exiting E_{ijkm}
DPT_{ijknm} = Dew point temperature (DPT) of hot stream i entering E_{ijkm}
dpt_{ijknm} = Dew point temperature (DPT) of cold stream j exiting E_{ijkm}
BPT_{ijknm} = Bubble point temperature (BPT) of hot stream i entering E_{ijkm}
bpt_{ijknm} = Bubble point temperature (BPT) of cold stream j exiting E_{ijkm}
DPH_{ijknm} = Dew point enthalpy of hot stream i entering E_{ijkm}
dph_{ijknm} = Dew point enthalpy of cold stream j exiting E_{ijkm}
BPH_{ijknm} = Bubble point enthalpy of hot stream i entering E_{ijkm}
bph_{ijknm} = Bubble point enthalpy of cold stream j exiting E_{ijkm}
T^{SH}_{ijknm} = Temperatures of hot stream i entering E_{ijkm} in the superheated zone
T^{TP}_{ijknm} = Temperatures of hot stream i entering E_{ijkm} in the two-phase zone
T^{SC}_{ijknm} = Temperatures of hot stream i entering E_{ijkm} in the subcooled zone
t^{SH}_{ijknm} = Temperatures for cold stream j exiting E_{ijkm} in the superheated zone
t^{TP}_{ijknm} = Temperatures for cold stream j exiting E_{ijkm} in the two-phase zone
t^{SC}_{ijknm} = Temperatures for cold stream j exiting E_{ijkm} in the subcooled zone
ΔT^{SH}_{ijknm}, ΔT^{TP}_{ijknm}, ΔT^{SC}_{ijknm} = Departures of zone temperatures of hot stream i entering E_{ijkm} from its boundary point temperatures (DPT and BPT)
Δt^{SH}_{ijknm}, Δt^{TP}_{ijknm}, Δt^{SC}_{ijknm} = Departures of zone temperatures of cold stream j exiting E_{ijkm} from its boundary point temperatures
ΔH^{SH}_{ijknm}, ΔH^{TP}_{ijknm}, ΔH^{SC}_{ijknm} = Departures of stream enthalpy of hot stream i entering E_{ijkm} from its boundary point enthalpies (DPH and BPH)
Δh^{SH}_{ijknm}, Δh^{TP}_{ijknm}, Δh^{SC}_{ijknm} = Departures of stream enthalpy of cold stream j exiting E_{ijkm} from its boundary point enthalpies
z^{SH}_{ijknm} = 0−1 continuous variable to compare the enthalpy of hot stream i entering E_{ijkm} and its dew point enthalpy
z^{SC}_{ijknm} = 0−1 continuous variable to compare the enthalpy of hot stream i entering E_{ijkm} and its bubble point enthalpy
y^{SH}_{ijknm} = 0−1 continuous variable to compare the enthalpy of cold stream j exiting E_{ijkm} and its dew point enthalpy
y^{SC}_{ijknm} = 0−1 continuous variable to compare the enthalpy of cold stream j exiting E_{ijkm} and its bubble point enthalpy
ΔT_{ijknm} = Temperature differences at the end points of E_{ijkm}
$AMTD_{ijknm}$ = Arithmetic mean of the temperature differences at the end points of E_{ijkm}
h^t_{in} = Film heat-transfer coefficient for hot stream i in data set n
h^s_{jn} = Film heat-transfer coefficient for cold stream j in data set n
U_{ijn} = Overall heat-transfer coefficient for E_{ijkm} in data set n
A_{ijknm} = Heat-transfer area for E_{ijkm}
A_{ijk} = Estimated heat-transfer area for E_{ijk}

REFERENCES

(1) Nagesh Rao, H.; Karimi, I. A. A superstructure-based model for multistream heat exchanger design within flow sheet optimization. *AIChE J.* **2017**, *63* (9), 3764−3777.
(2) Hasan, M. M. F.; Karimi, I. A.; Alfadala, H. E.; Grootjans, H. Operational modeling of multistream heat exchangers with phase changes. *AIChE J.* **2009**, *55* (1), 150−171.
(3) Lee, G. C.; Smith, R.; Zhu, X. X. Optimal Synthesis of Mixed-Refrigerant Systems for Low-Temperature Processes. *Ind. Eng. Chem. Res.* **2002**, *41* (20), 5016−5028.
(4) Bach, W.; Foerg, W.; Steinbauer, M.; Stockmann, R.; Voggenreiter, F. Spiral wound heat exchangers for LNG baseload plants. Presented in the *13th International Conference and Exhibition on Liquefied Natural Gas*, Seoul, South Korea, May 14−17, 2001; PS5-1.
(5) Kamath, R. S.; Biegler, L. T.; Grossmann, I. E. Modeling multistream heat exchangers with and without phase changes for simultaneous optimization and heat integration. *AIChE J.* **2012**, *58* (1), 190−204.
(6) Watson, H. A. J.; Khan, K. A.; Barton, P. I. Multistream heat exchanger modeling and design. *AIChE J.* **2015**, *61* (10), 3390−3403.
(7) Watson, H. A. J.; Barton, P. I. Modeling phase changes in multistream heat exchangers. *Int. J. Heat Mass Transfer* **2017**, *105*, 207−219.
(8) Watson, H. A. J.; Vikse, M.; Gundersen, T.; Barton, P. I. Reliable Flash Calculations: Part 2. Process Flowsheeting with Nonsmooth Models and Generalized Derivatives. *Ind. Eng. Chem. Res.* **2017**, *56* (50), 14848−14864.
(9) Vikse, M.; Watson, H. A. J.; Gundersen, T.; Barton, P. I. Versatile Simulation Method for Complex Single Mixed Refrigerant Natural Gas Liquefaction Processes. *Ind. Eng. Chem. Res.* **2018**, *57* (17), 5881−5894.
(10) Watson, H. A. J.; Vikse, M.; Gundersen, T.; Barton, P. I. Optimization of single mixed-refrigerant natural gas liquefaction processes described by nondifferentiable models. *Energy* **2018**, *150*, 860−876.
(11) Pattison, R. C.; Baldea, M. Multistream heat exchangers: Equation-oriented modeling and flowsheet optimization. *AIChE J.* **2015**, *61* (6), 1856−1866.
(12) Tsay, C.; Pattison, R. C.; Baldea, M. Equation-oriented simulation and optimization of process flowsheets incorporating detailed spiral-wound multistream heat exchanger models. *AIChE J.* **2017**, *63* (9), 3778−3789.
(13) Skaugen, G.; Hammer, M.; Wahl, P. E.; Wilhelmsen, Ø Constrained non-linear optimization of a process for liquefaction of natural gas including a geometrical and thermo-hydraulic model of a compact heat exchanger. *Comput. Chem. Eng.* **2015**, *73*, 102−115.
(14) Yee, T. F.; Grossmann, I. E.; Kravanja, Z. Simultaneous optimization models for heat integration—I. Area and energy targeting and modeling of multi-stream exchangers. *Comput. Chem. Eng.* **1990**, *14* (10), 1151−1164.
(15) Goyal, M.; Chakravarty, A.; Atrey, M. D. Two dimensional model for multistream plate fin heat exchangers. *Cryogenics* **2014**, *61*, 70−78.
(16) Skaugen, G.; Kolsaker, K.; Walnum, H. T.; Wilhelmsen, Ø. A flexible and robust modelling framework for multi-stream heat exchangers. *Comput. Chem. Eng.* **2013**, *49*, 95−104.
(17) Khan, M. S.; Husnil, Y. A.; Getu, M.; Lee, M. Modeling and Simulation of Multi-stream Heat Exchanger Using Artificial Neural Network. *Comput.-Aided Chem. Eng.* **2012**, *31*, 1196−1200.

DOI: 10.1021/acs.iecr.8b05270
Ind. Eng. Chem. Res. 2019, 58, 5838−5850

(18) Jiang, L.; Zhou, K.; Zhu, L. Equation-oriented Modeling of Multi-stream Heat Exchanger in Air Separation Units. *Comput.-Aided Chem. Eng.* **2015**, *37*, 371−376.
(19) Yee, T. F.; Grossmann, I. E. Simultaneous optimization models for heat integration—II. Heat exchanger network synthesis. *Comput. Chem. Eng.* **1990**, *14* (10), 1165−1184.
(20) Hasan, M. M. F.; Jayaraman, G.; Karimi, I. A.; Alfadala, H. E. Synthesis of heat exchanger networks with nonisothermal phase changes. *AIChE J.* **2010**, *56* (4), 930−945.
(21) Chen, J. J. J. Comments on improvements on a replacement for the logarithmic mean. *Chem. Eng. Sci.* **1987**, *42* (10), 2488−2489.
(22) Paterson, W. R. A Replacement for the Logarithmic Mean. *Chem. Eng. Sci.* **1984**, *39*, 1635−1636.
(23) Wang, M.; Zhang, J.; Xu, Q. Optimal design and operation of a C3MR refrigeration system for natural gas liquefaction. *Comput. Chem. Eng.* **2012**, *39*, 84−95.

DOI: 10.1021/acs.iecr.8b05270
Ind. Eng. Chem. Res. 2019, 58, 5838−5850